Supporting Information

Bi-Synergistic Ligand-Mediated Passivation of Surface Defects for Highly Efficient and Stable Cesium-Lead-Iodide Perovskite Quantum Dot Photovoltaics

*Minju Yang[a], Seon Joong Kim[a], Tae Hyuk Kim[a], Hyungju Ahn[b], Min Jong Lee[a], Yunsang Kim[c], and Jae Won Shim[a]**

[a]School of Electrical Engineering, Korea University, 145, Anam-ro, Seongbuk-gu, Seoul, 02841, Republic of Korea
[b]Industry Technology Convergence Center, Pohang Accelerator Laboratory, Pohang 37673, Republic of Korea
[c]Department of Sustainable Bioproducts, Mississippi State University, Starkville, MS 39759 USA

**E-mail*: jwshim19@korea.ac.kr

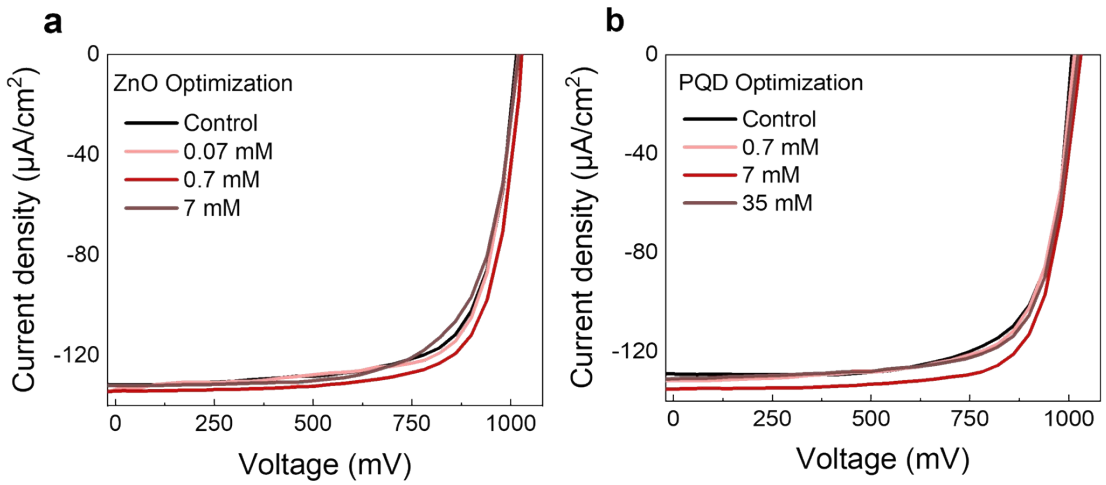

Figure S1. *J-V* characteristics for the TFMBA concentration optimization. (a) Optimization of TFMBA concentration (0.07, 0.7, and 7 mM) for the ZnO layer passivation. (b) Optimization of TFMBA concentration (0.7, 7, and 35 mM) for the PQD layer passivation.

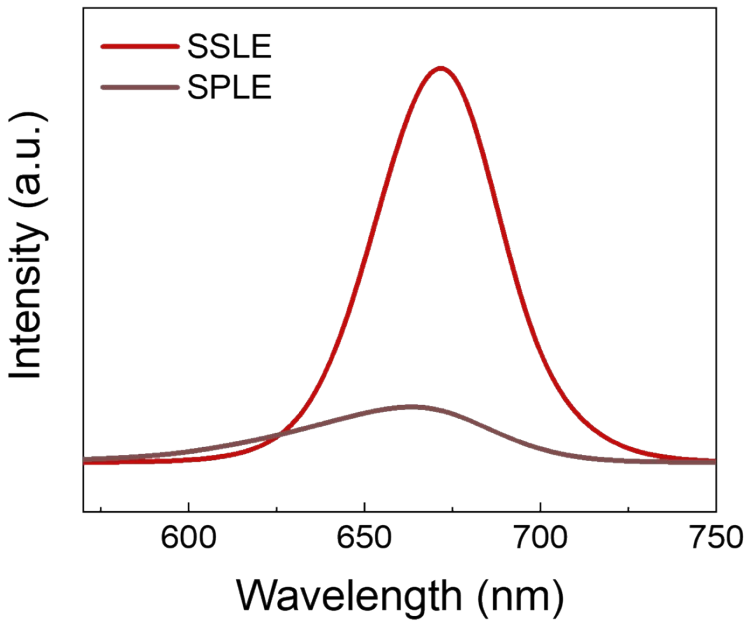

Fig. S2. PL spectra of the pristine and TFMBA-treated $CsPbI_3$ PQD solutions, confirming material degradation after the SPLE attempt.

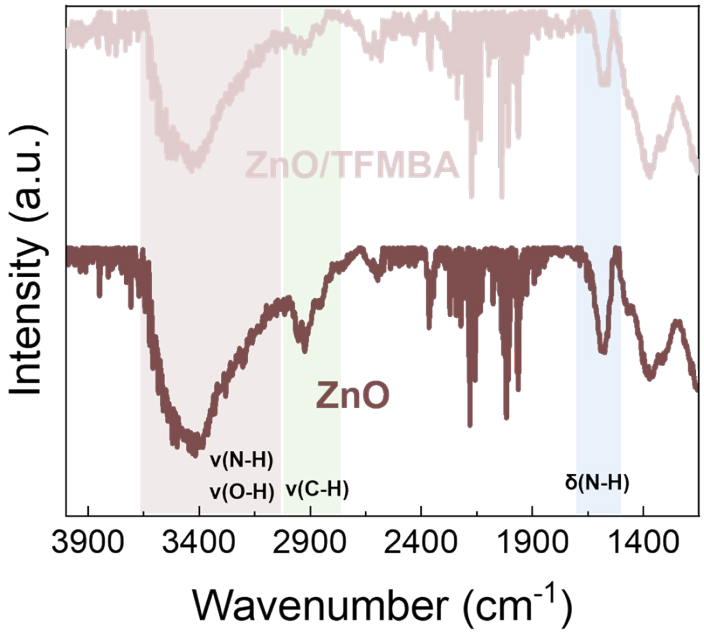

Fig. S3. FT-IR spectra of the pristine ZnO and ZnO/TFMBA films.

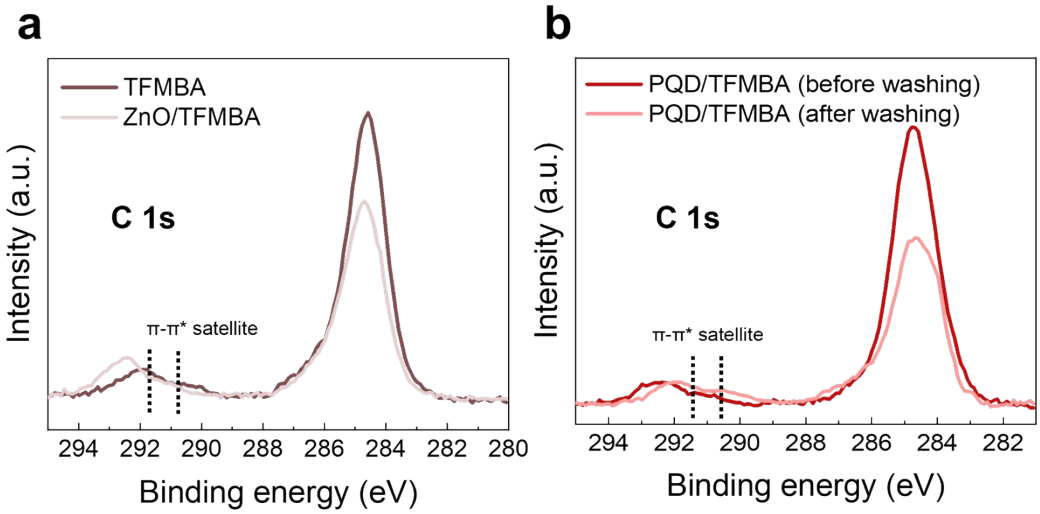

Fig. S4. C 1s XPS spectra of (a) the TFMBA and ZnO/TFMBA films, and (b) the PQD/TFMBA films recorded before and after the MeOAc washing step.

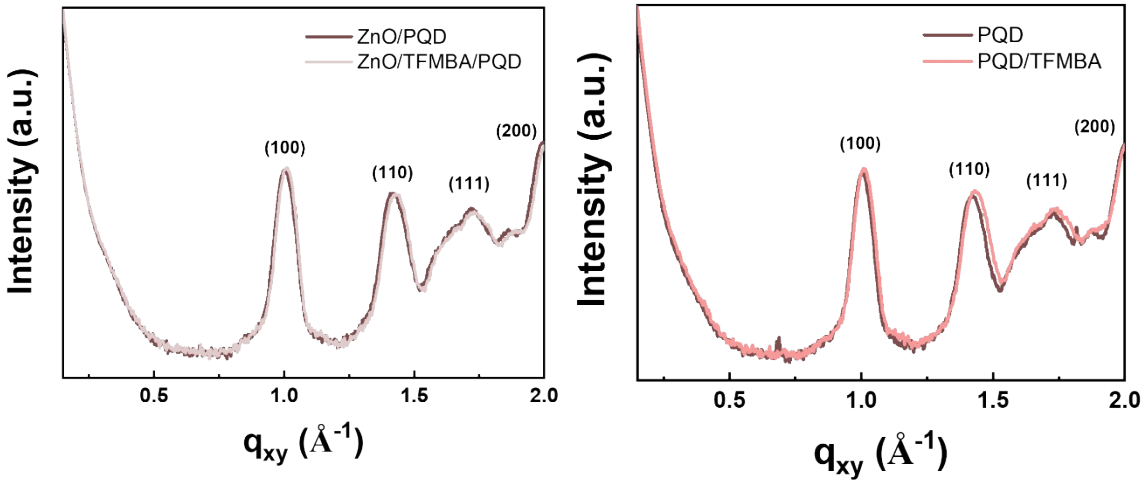

Fig. S5. Radial line profiles of the ZnO/PQD and ZnO/TFMBA/PQD films. The corresponding results for the PQD films before and after TFMBA passivation are also shown, exhibiting consistent PQD diffraction peaks corresponding to the (100), (110), (111), and (200) planes.

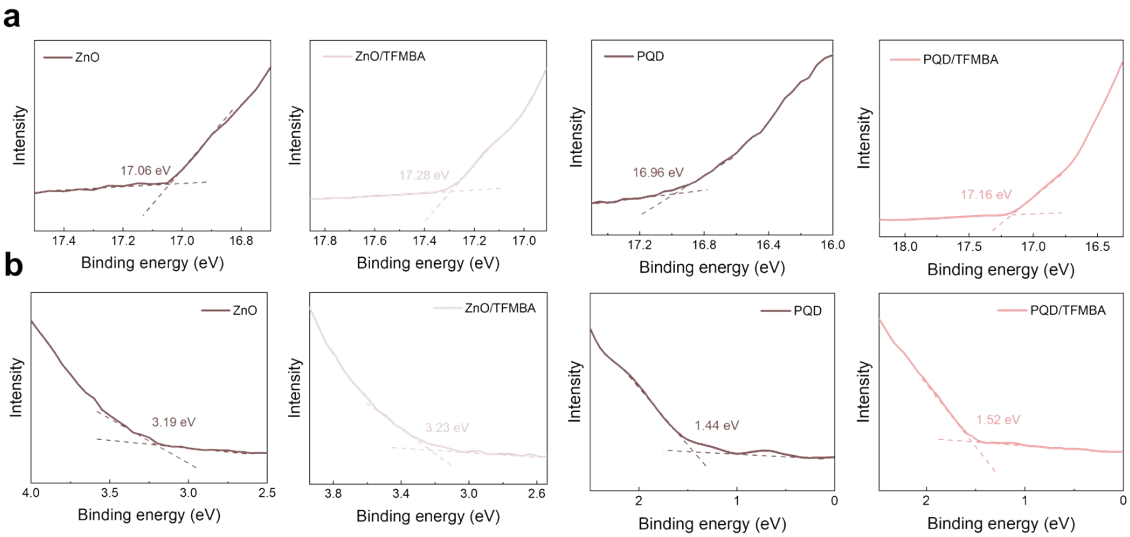

Fig. S6. UPS spectra recorded for the ZnO, ZnO/TFMBA, PQD, PQD/TFMBA films, showing (a) the secondary electron cut-off regions and (b) the valence band edge onsets before and after ligand treatment.

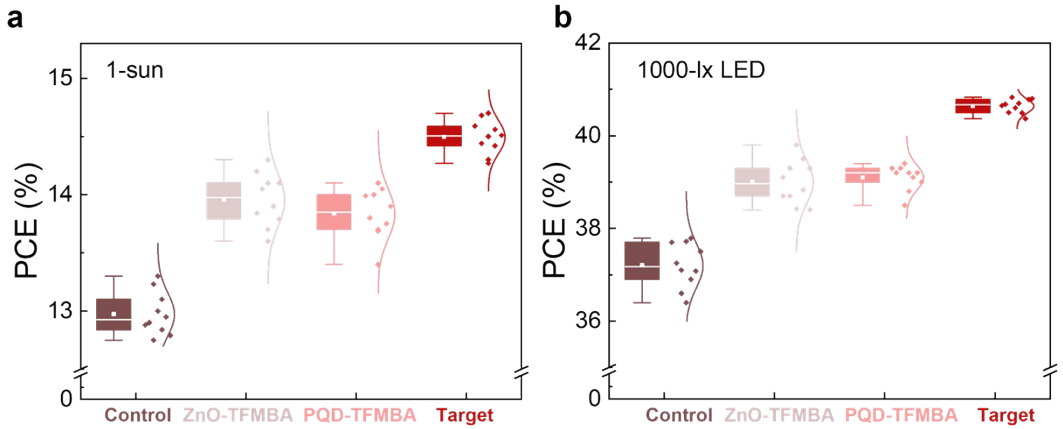

Fig. S7. Statistical distributions of the PCE for the control, ZnO–TFMBA, PQD–TFMBA, and target devices under (a) 1-sun illumination (AM1.5G, 100 mW cm^{-2}) and (b) LED illumination (1000-lx, 0.254 mW cm^{-2}).

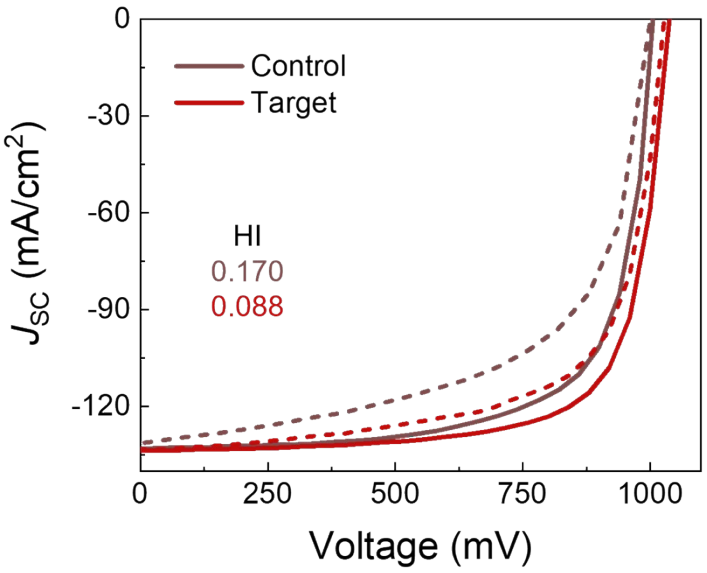

Fig. S8. HIs of the control and target devices extracted from the reverse (solid lines) and forward (dashed lines) *J-V* scans.

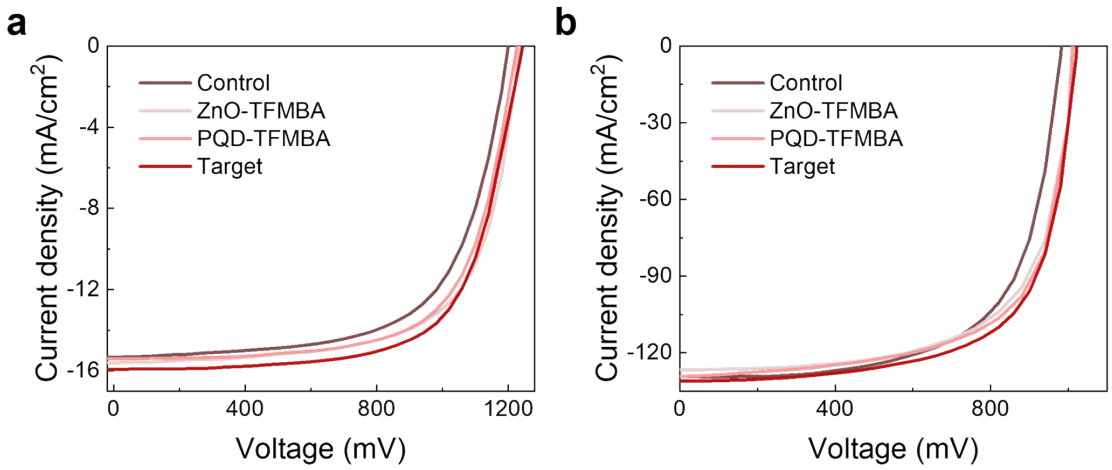

Fig. S9. *J-V* curves of the champion large-area (1.0 cm^2) device measured under (a) 1-sun and (b) 1000-lx LED illumination.

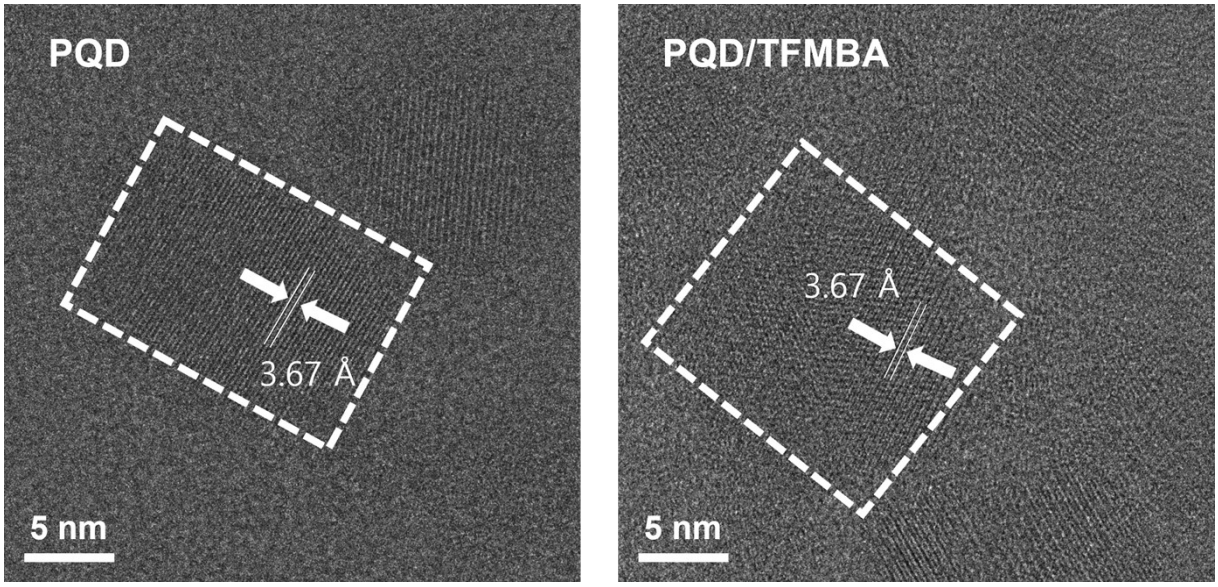

Fig. S10. High-resolution TEM images recorded for the PQD films before and after TFMBA passivation.

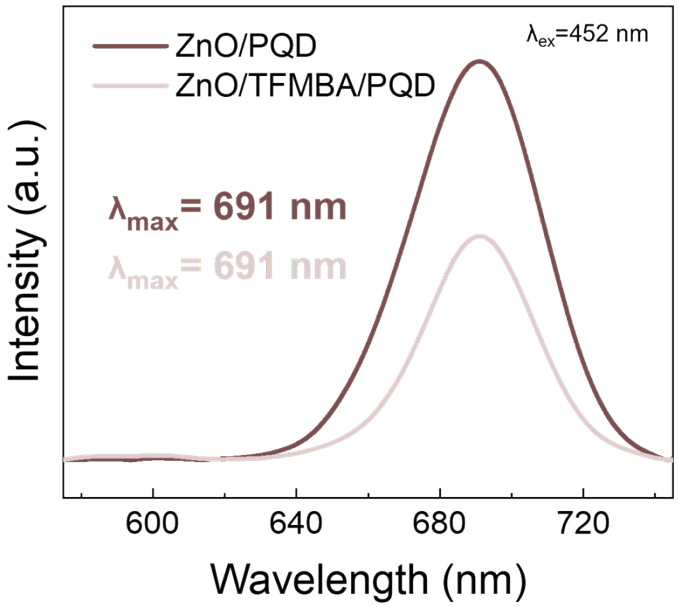

Fig. S11. Steady-state PL spectra recorded for the ZnO/PQD and ZnO/TFMBA/PQD films (excitation wavelength: 452 nm).

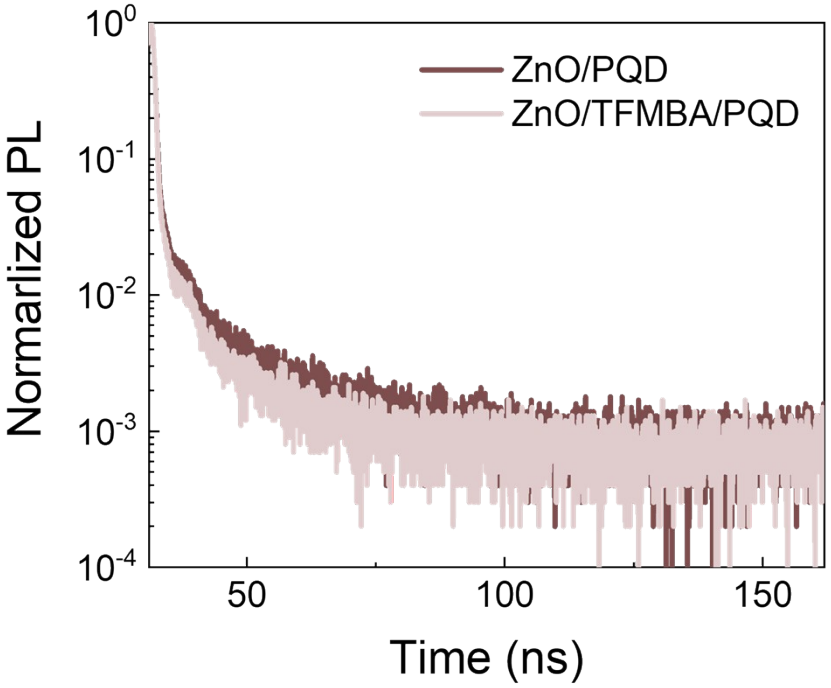

Fig. S12. TRPL decay curves recorded for the ZnO/PQD and ZnO/TFMBA/PQD films.

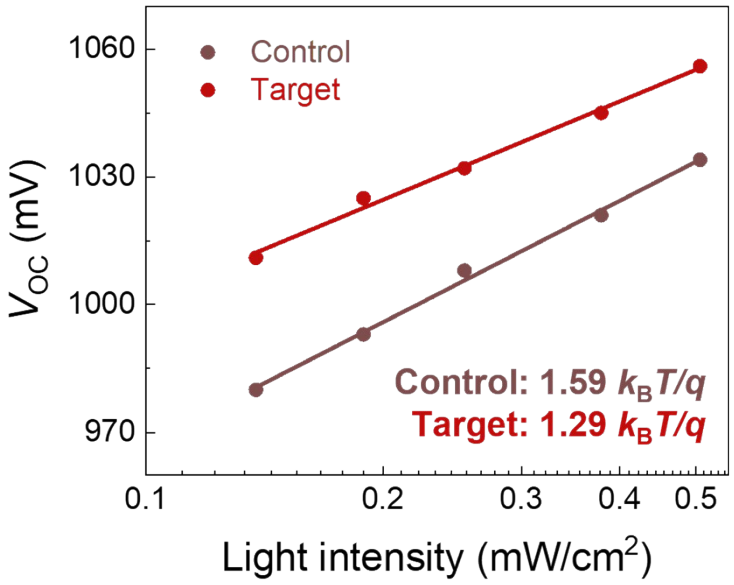

Fig. S13. Dependence of V_{OC} on the incident light intensity under LED illumination for the control and target devices.

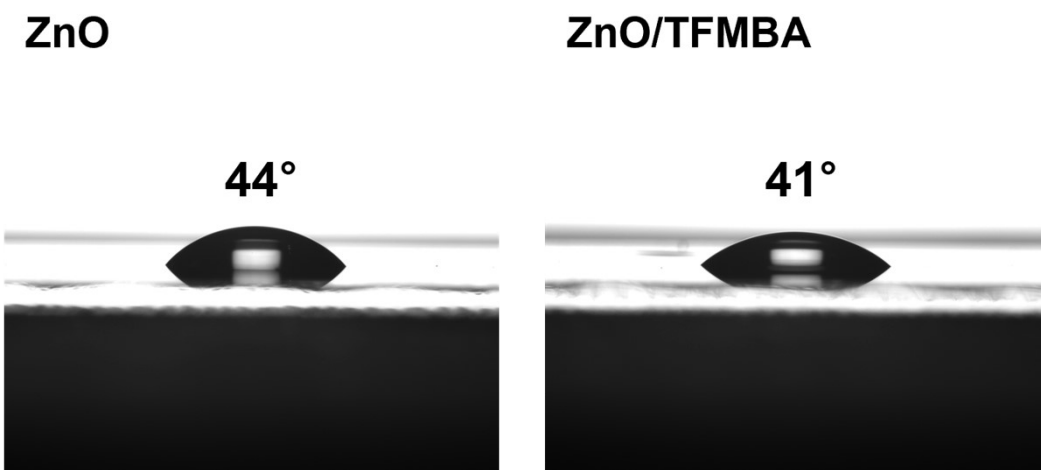

Fig. S14. Contact angles of the ZnO and ZnO/TFMBA films.

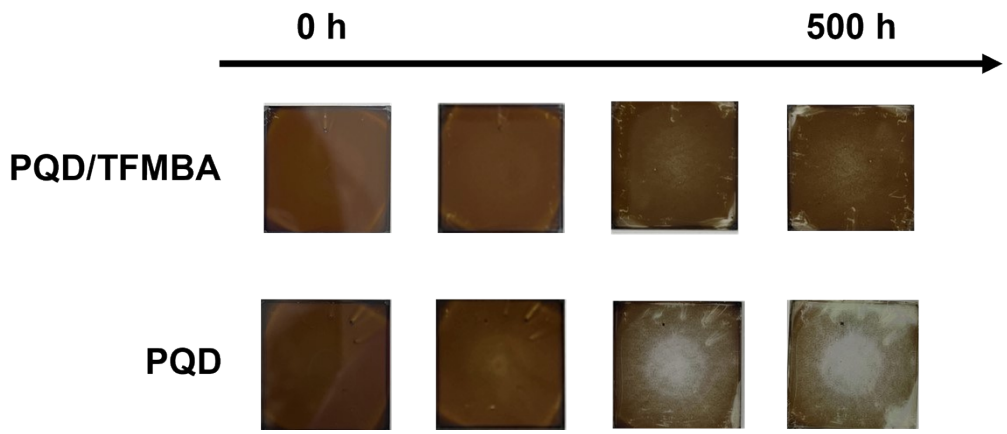

Fig. S15. Photographs of the PQD films with and without TFMBA treatment after ambient aging (20%–30% RH) for different durations.

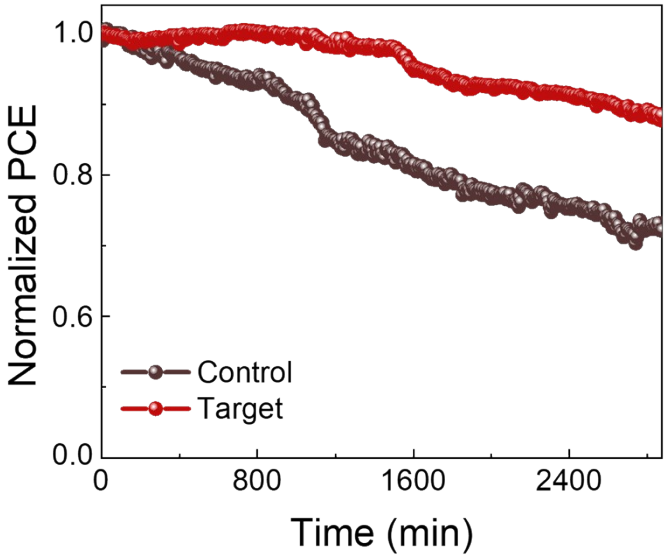

Figure S16. PCE retention of the control and target devices under continuous MPP tracking under 20%–30% RH.

Table S1. Relative fractions of lattice O, O vacancies, and hydroxyl groups derived from deconvolution of the O 1s XPS spectra recorded for the ZnO and ZnO/TFMBA films.

	Lattice O [%]	O vacancies [%]	Hydroxyl groups [%]
ZnO	48.3	28.1	23.6
ZnO/TFMBA	54.9	26.5	18.6

Table S2. PV performance of the large-area (1.0 cm^2) devices under 1000-lx LED illumination.

	V_{OC} [mV]	J_{SC} [μA/cm^2]	FF [%]	PCE [%]
Control	982.2	127.9	66.37	32.8
ZnO-TFMBA	1010.2	126.7	66.67	33.6
PQD-TFMBA	1011.7	129.2	66.86	34.4
Target	1022.0	131.0	67.42	35.5

Table S3. PV performance of the large-area (1.0 cm^2) devices under 1-sun illumination.

	V_{OC} [mV]	J_{SC} [mA/cm^2]	FF [%]	PCE [%]
Control	1199.7	15.3	65.0	11.9
ZnO-TFMBA	1226.3	15.6	66.8	12.8
PQD-TFMBA	1230.2	15.4	67.3	12.7
Target	1242.9	15.9	68.1	13.5